Article

Chinese Science Bulletin

Astronomy

December 2013 Vol.58 No.36: 4588–4592
doi: 10.1007/s11434-013-6097-3

Photometric modeling of the Moon using Lommel-Seeliger function and Chang'E-1 IIM data

ZHANG Jiang[1,2*], LING ZongCheng[2], ZHANG WenXi[3], REN Xin[4], LI ChunLai[4] & LIU JianZhong[5]

[1] *School of Physics, Shandong University, Jinan 250100, China;*
[2] *School of Space Science and Physics & Shandong Provincial Key Laboratory of Optical Astronomy & Solar-Terrestrial Environment, Shandong University, Weihai 264209, China;*
[3] *Academy of Opto-Electronics, Chinese Academy of Sciences, Beijing 100094, China;*
[4] *National Astronomical Observatories, Chinese Academy of Sciences, Beijing 100012, China;*
[5] *Institute of Geochemistry, Chinese Academy of Sciences, Guiyang 550002, China*

Received July 4, 2013; accepted October 12, 2013

The imaging interferometer (IIM) aboard the Chang'E-1 lunar orbiter is the first multispectral imaging spectrometer for Chinese lunar missions. Before science applications (e.g., FeO and TiO_2 mapping) of the IIM raw data, the radiance variation due to changes in illumination and viewing geometry has to be removed from the radiometrically calibrated IIM Level 2A images. To achieve this, we fit the IIM Level 2A radiance data with a Lommel-Seeliger photometric model consisting of an exponential term and a fourth order polynomial in the phase function, without distinguishing between lunar maria and highlands. The exponential and the fourth order polynomial parameters are derived separately by fitting to two datasets divided at a solar phase angle threshold, avoiding a decrease in the phase function close to zero phase angle. Different phase angle thresholds result in coincident fitting curves between 20° and 75°, while large discrepancies occur at other phase angles. Then the derived photometric model is used to normalize the IIM Level 2A data to radiance values at an incidence and phase angle of 30° and emission angle of 0°. Our photometric model is validated by comparing two photometrically normalized IIM radiance spectra covering the same areas, showing a relative deviation consistent with the IIM preflight calibration.

Chang'E-1, IIM, Lommel-Seeliger, photometric model

Citation: Zhang J, Ling Z C, Zhang W X, et al. Photometric modeling of the Moon using Lommel-Seeliger function and Chang'E-1 IIM data. Chin Sci Bull, 2013, 58: 4588–4592, doi: 10.1007/s11434-013-6097-3

The Chang'E-1, the first Chinese lunar orbiter launched in 2007, is equipped with eight payloads [1], achieving a variety of scientific results [2–7]. The imaging interferometer (IIM), one of the eight payloads aboard the Chinese Chang' E-1 lunar orbiter, is a Sagnac-based push-broom imaging spectrometer designed to acquire 32-band multispectral observations over the spectral range 480–960 nm and map mineralogical and elemental compositions on the surface of the Moon. It obtained 706 orbits of images through the mission duration from November, 2007 to March, 2009, covering 84% of the lunar surface between 70°S and 70°N at a spatial resolution of 200 m/pixel and with a solar phase angle range of 0°–80° [1]. To compare multispectral observations under varying illumination-viewing geometries, produce image mosaics, and enable lunar mineralogical and elemental mapping [8], a lunar photometric model must be developed to normalize the IIM data to a standard geometry. Chen et al. [9] calculated Lommel-Seeliger model parameters using 261 orbits of the IIM data, resulting in a decreasing phase function when approaching small phase angles. Wu et al. [10] developed Lommel-Seeliger and fourth order polynomial photometric functions for four classes of terrain

*Corresponding author (email: zhang_jiang@sdu.edu.cn)

types with different FeO contents, using part of the IIM data (Orbit 2217–3000) that are converted to reflectance. In order to derive a Lommel-Seeliger photometric model based on all of the IIM data for global use, remove its variation due to changes in illumination-viewing geometry by photometric normalization, and avoid extra uncertainties introduced by data processing steps such as reflectance calculation and FeO inversion, we fit the Lommel-Seeliger model to all of the IIM Level 2A data divided at a variety of solar phase angle thresholds, and test the photometric model with two photometrically normalized IIM radiance spectra covering the same area.

1 IIM data

The IIM raw data are converted to Level 2A radiance images through data preprocessing pipeline and radiometric calibration; the illumination-viewing geometry for each pixel in radiance images is calculated from the Chang'E-1 navigation and IIM pointing data. To increase signal-to-noise ratio and reduce computation time, data points are collected from the IIM Level 2A images in an approach similar to that described in [11]:

(1) In each orbit of image, pixels at a solar phase angle larger than 20° are binned into 32×32 blocks for each spectral band; those with solar phase angles lower than 20° are binned into 16×16 blocks to account for lunar opposition effect.

(2) Radiance is averaged over each block, and incidence, emission, and phase angles at central pixel are retrieved as the illumination-viewing geometry.

(3) The averaged radiance is divided by the corresponding Lommel-Seeliger factor $\mu_0/(\mu_0+\mu)$ for the central pixel in each block to correct limb-darkening, where μ_0, μ are cosine values of the incidence and emission angles for the central pixel, respectively.

This reduced dataset consists of 2.06 millions of spatially resampled radiance spectra corrected for limb-darkening and corresponding illumination-viewing geometries. Although lunar maria and highlands exhibit distinct photometric behaviors [11], as a first order approximation, we follow the approach by McEwen [12] that data points for these two lunar terrain types are not distinguished to fit photometric models in photometric normalization.

2 Lommel-Seeliger model

Lunar photometric models describe how the solar radiation reflected by the lunar surface varies with illumination-viewing geometry defined by incidence angle i, emission angle e, and solar phase angle α as described in [13]. For low albedo solar system bodies such as the Moon, single scattering dominates in the regolith, and except close to zero solar phase angle, lunar surface radiance $I(i,e,\alpha)$ can be well approximated by the Lommel-Seeliger Law [13]:

$$I(i,e,\alpha)=\frac{\mu_0}{\mu_0+\mu}f(\alpha), \tag{1}$$

where $f(\alpha)$ describes the radiance variation due to solar phase angle alone, and contains all the model parameters. One of the simplest empirical expressions for $f(\alpha)$ in eq. (1) is a fourth order polynomial plus an exponential term [11]:

$$f(\alpha)=b_0e^{-b_1\alpha}+a_0+a_1\alpha+a_2\alpha^2+a_3\alpha^3+a_4\alpha^4, \tag{2}$$

where the exponential term is added to account for lunar opposition effect close to zero solar phase angle. For its simplicity and adequate accuracy, eq. (2) has been widely used in the photometric normalization for the imaging spectrometers aboard the most recent lunar orbital missions such as the lunar reconnaissance orbiter wide angle camera and the Moon mineralogy mapper [14,15].

The best fit of eq. (2) to the spatially resampled and limb darkening corrected IIM data (α_j, f_j) is found to minimize the χ^2:

$$\chi^2=\sum_j\left[f_j-f\left(\alpha_j\right)\right]^2. \tag{3}$$

The model parameters minimizing the χ^2 in eq. (3) are obtained using routines implemented with Levenberg-Marquardt algorithm such as IDL® routine LMFIT, MPFIT (http://cow.physics.wisc.edu/~craigm/idl/), and Fortran package Minpack (http://www.netlib.org/minpack). These routines are first tested against the StRD datasets (http://www.itl.nist.gov/div898/strd) used to evaluate nonlinear least squares procedures, indicating Minpack is more accurate and reliable.

The cumulative histogram of the solar phase angle (Figure 1) suggests the data points of low phase angle (α<15°) is no more than 20% of the whole spatially resampled IIM radiance dataset; therefore, the main contribution to the χ^2 may come from those of large phase angle, and the exponential term accounting for lunar opposition effect in eq. (2)

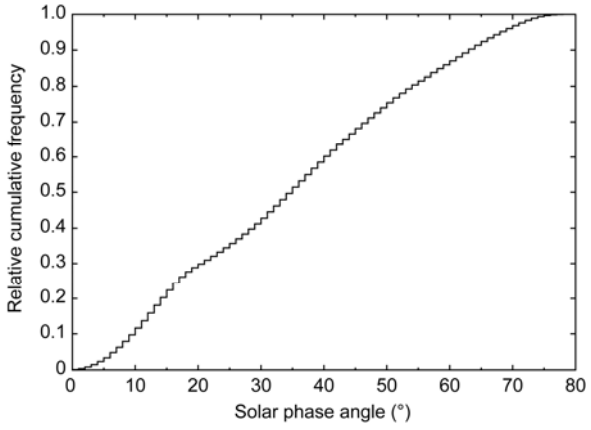

Figure 1 Relative cumulative histogram of the solar phase angle for the spatially resampled IIM data.

cannot be well constrained by minimizing the χ^2 in eq. (3), resulting in a decrease in $f(\alpha)$ close to zero solar phase angle when the Lommel-Seeliger model is fitted with the whole dataset using Minpack (Figure 2). To avoid this decrease, first we fit the exponential plus constant terms in eq. (2) to the data points at solar phase angle lower than a threshold α_0, with initial parameter values in Table 1; then with b_0 and b_1 fixed, eq. (2) is fitted to the data points of $\alpha>\alpha_0$, using initial parameter values from the order of a fourth-order polynomial fit to the data points of $\alpha>\alpha_0$ (Table 1).

3 Results

As shown in Figure 2, the Lommel-Seeliger model fit to the IIM data varies with a change in phase angle threshold α_0,

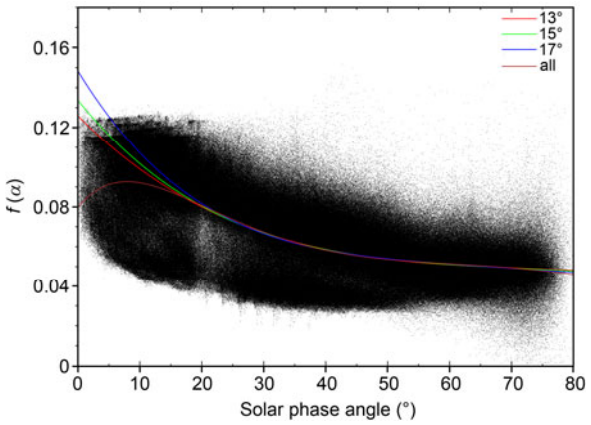

Figure 2 (Color online) Lommel-Seeliger function fits to the IIM band 24 (757 nm) spatially resampled and limb-darkening-corrected radiance data at solar phase angle thresholds α_0=13°, 15° and 17° and for all solar phase angles.

Table 1 Initial parameter values for the Lommel-Seeliger fit to the IIM spatially resampled and limb-darkening-corrected radiance data

b_0	b_1	a_0	a_1 (10^{-3})	a_2 (10^{-4})	a_3 (10^{-5})	a_4 (10^{-7})
Exponential and constant terms						
0.1	0.1	0.1				
Order of fourth order polynomial fit to the IIM data						
			1.0	−1.0	1.0	−1.0

particularly at solar phase angles lower than 20° and larger than 75°; however, the fitting curves between 20°and 75°are barely affected. As lunar opposition effect should be significantly reduced at α>15° [11], the Lommel-Seeliger model fit at phase angle threshold α_0=15° (Table 2) is selected as our preliminary result. This Lommel-Seeliger model is validated by photometric normalization, in which the radiance value $I(i,e,\alpha)$ at each pixel of the IIM Level 2A images are normalized to a standard geometry of incidence and phase angle of 30° and emission angle of 0° by [12]

$$I(30°,0°,30°)=\frac{\cos 30°}{\cos 30°+\cos 0°}\frac{\cos i+\cos e}{\cos i}\frac{f(30°)}{f(\alpha)}I(i,e,\alpha). \quad (4)$$

For two IIM radiance spectra covering the same area, their deviation is caused by different illumination-viewing geometries (Figure 3) and they should be equal after photometric normalization by a perfect photometric model. To validate the derived photometric function, we select 7 homogenous and flat areas as validation sites (Table 3), with various illumination-viewing geometries, albedo and terrain types. As shown in Figures 4 and 5, the relative deviation between two photometrically normalized spectra covering the same area is consistent with the uncertainty (15%)

Table 2 The Lommel-Seeliger model fit to the IIM Level 2A radiance data with a solar phase angle threshold of 15°. The fit to the noisy IIM band 32 data cannot converge and is not used

Band	Wavelength (nm)	b_0	b_1 (10^{-4})	a_0	a_1 (10^{-3})	a_2 (10^{-5})	a_3 (10^{-7})	a_4 (10^{-9})
1	480.914286	1.4706	1.8967	−1.2922	−4.1831	6.8548	−5.4089	2.4093
2	488.670968	2.3905	1.1687	−2.2180	−4.3306	7.4086	−5.9329	2.2723
3	496.681967	2.7012	1.0415	−2.5346	−4.2270	7.2512	−5.6915	2.0312
4	504.960000	3.1656	0.92796	−3.0063	−4.0833	7.1312	−5.5687	1.8719
5	513.518644	3.0609	8.7780	−2.9188	−3.6757	6.4985	−5.1042	1.6930
6	522.372414	2.8839	8.7941	−2.7486	−3.5321	6.3092	−5.0130	1.6621
7	531.536842	2.7197	9.2238	−2.5806	−3.6309	6.4752	−5.1558	1.7133
8	541.028571	2.5352	9.5747	−2.3916	−3.7556	6.6879	−5.3642	1.8063
9	550.865455	2.8573	10.302	−2.6787	−4.6840	8.3028	−6.5030	2.0633
10	561.066667	2.8639	9.9055	−2.6959	−4.4213	7.8966	−6.2132	1.9652
11	571.652830	2.5374	1.0021	−2.3837	−4.0760	7.3357	−5.8296	1.8515
12	582.646154	2.3550	1.0136	−2.1999	−4.1292	7.4309	−5.9640	1.9282
13	594.070588	2.4657	1.0659	−2.2818	−4.8662	8.6074	−6.7281	2.0886
14	605.952000	2.1021	1.1053	−1.9286	−4.6516	8.2865	−6.5216	1.9954
15	618.318367	2.0388	1.0822	−1.8729	−4.4977	8.0754	−6.4228	1.9686

(*To be continued on the next page*)

(*Continued*)

Band	Wavelength (nm)	b_0	b_1 (10^{-4})	a_0	a_1 (10^{-3})	a_2 (10^{-5})	a_3 (10^{-7})	a_4 (10^{-9})
16	631.200000	1.8596	1.0471	−1.6959	−4.4464	7.9912	−6.3845	1.9643
17	644.629787	1.5478	1.1188	−1.3825	−4.5158	8.0811	−6.4241	1.9412
18	658.643478	1.1770	1.2402	−1.0271	−4.1263	7.4486	−6.0190	1.8575
19	673.280000	1.1531	1.1913	−0.99252	−4.4198	7.9243	−6.3665	1.9390
20	688.581818	0.81606	1.3285	−0.66638	−4.1521	7.4591	−6.0392	1.8486
21	704.595349	0.69964	1.4195	−0.54886	−4.1757	7.4965	−6.0946	1.8814
22	721.371429	0.51068	1.4878	−0.36692	−3.9936	7.1465	−5.8097	1.7842
23	738.965854	0.39334	1.6790	−0.25578	−3.8415	6.9088	−5.6597	1.7498
24	757.440000	0.13058	2.5022	−0.003139	−3.7829	6.8150	−5.6322	1.7450
25	776.861538	0.12702	2.4087	−0.01197	−3.9396	7.1101	−5.8711	1.8048
26	797.305263	0.05933	2.7639	0.06965	−3.7067	6.7497	−5.6531	1.7584
27	818.854054	−0.008633	1.2531×10^{6}	0.01290	−3.7396	6.8282	−5.7587	1.7988
28	841.600000	−0.008221	1.2096×10^{6}	0.1231	−3.5845	6.5998	−5.6111	1.7608
29	865.645714	−0.0072398	1.1772×10^{6}	0.1091	−3.2077	5.9949	−5.1905	1.6641
30	891.105882	−0.0074328	1.1324×10^{6}	0.1118	−3.2853	6.1330	−5.2904	1.6828
31	918.109091	−0.0034994	1.1022×10^{6}	0.5257	−1.5439	3.0440	−2.9387	1.1344

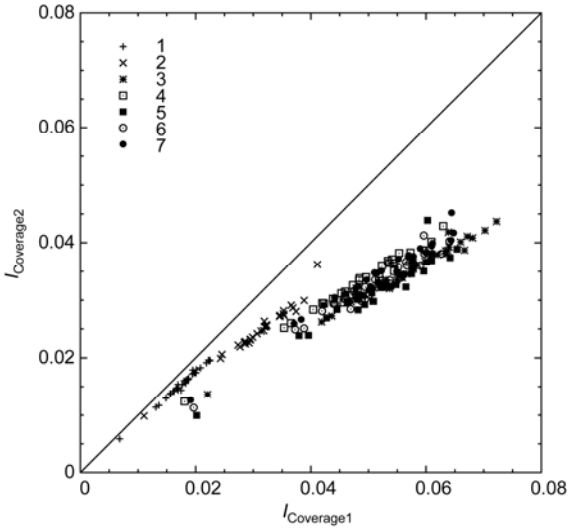

Figure 3 Scatter plot between two IIM 2A radiance spectra covering the same area and at different illumination-viewing geometries. These spectra are collected from 7 areas as listed in Table 3. The straight line denotes the two spectra are equal.

Table 3 Homogenous and flat validation areas. Each area is covered by two IIM images. Pixel locations refer to the upper left corner

Area	Coverage 1				Coverage 2				Size (Pixel)
	Orbit	Sample	Line	α	Orbit	Sample	Line	α	
1	2272	74	8341	34.9	2891	92	15608	42.3	7
2	2356	18	4180	38.6	2975	35	5828	46.9	10
3	2356	80	7736	17.2	2975	105	9435	41.9	10
4	2626	116	10131	16.1	2935	43	9275	33.3	10
5	2626	77	10332	12.9	2935	5	9479	30.0	10
6	2626	94	10859	11.8	2935	22	10005	30.5	9
7	2626	111	10999	12.6	2935	39	10145	31.8	10

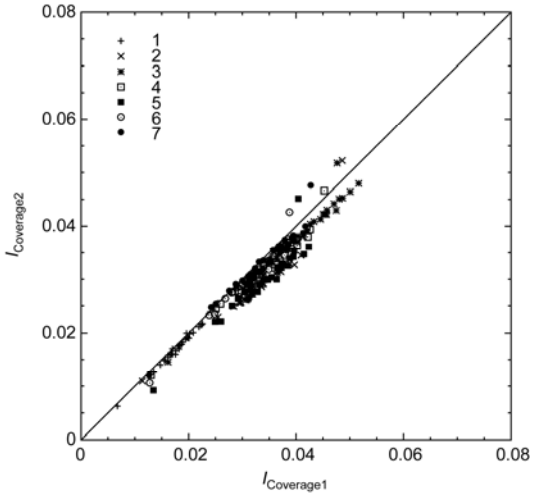

Figure 4 Scatter plot between two IIM 2A radiance spectra covering the same area and photometrically normalized to a standard illumination-viewing geometry. The straight line denotes the two normalized spectra are equal.

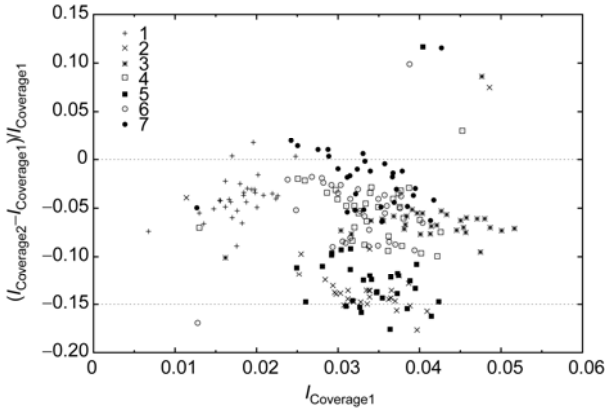

Figure 5 Relative deviation between two IIM 2A radiance spectra covering the same area and photometrically normalized to a standard illumination-viewing geometry. Most of data points lie within a relative deviation of 15%.

expected from the IIM preflight calibration [16].

4 Conclusions and future work

We derived a modified lunar Lommel-Seeliger photometric model consisting of an exponential term and a fourth-order polynomial in the phase function based on the IIM Level 2A radiance data. Preliminary validation by comparing two photometrically normalized spectra covering the same area suggests their relative deviation agrees with the IIM preflight calibration result.

However, our preliminary photometric model also has limitations, e.g., it is not fitted with separated lunar maria and highlands data as in [11,14]. In the future work, a global Chang'E-1 IIM mosaic will be made to collected data separately for these two lunar terrains, to select more overlapping areas from this mosaic for validation, and then to refine our lunar photometric model.

This work was supported by the National Natural Science Foundation of China (11003012, 41373068), the Natural Science Foundation of Shandong Province (ZR2011AQ001), Joint Funds of the National Natural Science Foundation of China and the Chinese Academy of Sciences (U1231103), Independent Innovation Foundation of Shandong University (2013ZRQP004).

1 Ouyang Z Y, Li C L, Zou Y L, et al. The primary science result from Chang'E-1 probe (in Chinese). Sci China Earth Sci (Chin Ver), 2010, 40: 261–280
2 Huang Y, Hu X G, Zhang X Z, et al. Improvement of orbit determination for geostationary satellites with VLBI tracking. Chin Sci Bull, 2011, 56: 2765–2772
3 Ling Z C, Zhang J, Liu J Z, et al. Preliminary results of TiO_2 mapping using imaging interferometer data from Chang'E-1. Chin Sci Bull, 2011, 56: 2082–2087
4 Jin Y Q, Fa W Z. The modeling analysis of microwave emission from stratified media of non-uniform lunar cratered terrain surface for Chinese Chang-E 1 observation. Chin Sci Bull, 2011, 56: 1165–1171
5 Fa W Z, Jin Y Q. Global inventory of Helium-3 in lunar regoliths estimated by a multi-channel microwave radiometer on the Chang-E 1 lunar satellite. Chin Sci Bull, 2010, 55: 4005–4009
6 Li J L, Guo L, Qian Z H, et al. Determination of the controlled landing trajectory of Chang'E-1 satellite and the coordinate analysis of the landing point on the Moon. Chin Sci Bull, 2010, 55: 1240–1245
7 Ping J S, Huang Q, Su X L, et al. Chang'E-1 orbiter discovers a lunar nearside volcano: YUTU mountain. Chin Sci Bull, 2009, 54: 4534–4536
8 Ling Z C, Zhang J, Liu J Z, et al. Preliminary results of FeO mapping using imaging interferometer data from Chang'E-1. Chin Sci Bull, 2011, 56: 376–379
9 Chen C, Qin Q M, Zhang N, et al. Research on photometric calibration and reflectance calculation of CE-1 IIS data (in Chinese). Spectrosc Spect Anal, 2011, 31: 1985–1990
10 Wu Y Z, Besse S, Li J Y, et al. Photometric correction and in-flight calibration of Chang'E-1 interference imaging spectrometer (IIM) data. Icarus, 2011, 222: 283–295
11 Hillier J K, Buratti B J, Hill K. Multispectral photometry of the Moon and absolute calibration of the Clementine UV/Vis camera. Icarus, 1999, 141: 205–225
12 McEwen A S. A precise lunar photometric function. Proc Lunar Planet Sci Conf, 1996, 27: 841–842
13 Hapke B W. Theory of reflectance and emittance spectroscopy. New York: Cambridge University Press, 1993
14 Denevi B W, Robinson M S, Hapke B W, et al. Global ultraviolet through visible color observations of the Moon with the lunar reconnaissance orbiter wide angle camera. Lunar and Planetary Science Conference Abstracts, 2010, 41: 2263
15 Hicks M D, Buratti B J, Staid M, et al. A visible and infrared spectrophotometric model for the Moon based on ROLO and Chandrayaan-1 Moon Mineralogy Mapper data. Lunar and Planetary Science Conference Abstracts, 2010, 41: 2076
16 Qiu Y H, Zhao B C, Zhao J K, et al. Field performance test experiments of the interference imaging spectrometer of Chang'E-1 satellite (in Chinese). Acta Photonica Sin, 2009, 38: 484–488